Depletion and Voids Formation in the Substrate During High Temperature Oxidation of Ni–Cr Alloys

Clara Desgranges · Florence Lequien · Edwige Aublant · Maylise Nastar · Daniel Monceau

Abstract A numerical model to treat the kinetics of vacancy annihilation at the metal/oxide interface but also in the bulk metal has been implemented. This was done using EKINOX, which is a mesoscopic scale 1D-code that simulates oxide growth kinetics with explicit calculation of vacancy fluxes. Calculations were performed for high temperature Ni–Cr alloys oxidation forming a single chromia scale. The kinetic parameters used to describe the diffusion in the alloy were directly derived from an atomistic model. Our results showed that the Cr depletion profile can be strongly affected by the cold work state of the alloy. In fact, the oversaturation of vacancies is directly linked to the efficiency of the sinks which is proportional to the density of dislocations. The resulting vacancy profile highlights a supersaturation of vacancy within the metal. Based on the classical nucleation theory, the possibility and the rate of void formation are discussed.

C. Desgranges (✉) · F. Lequien
CEA, DEN, DPC, SCCME, Laboratoire d'Etude de la Corrosion Non Aqueuse,
91191 Gif-sur Yvette, France
e-mail: clara.desgranges@cea.fr

F. Lequien
e-mail: florence.lequien@cea.fr

E. Aublant
AREVA-NP, Technical Center, 30 Bd de l'Industrie, 71205 Le Creusot Cedex, France
e-mail: edwige.aublant@areva.fr

M. Nastar
CEA, DEN, DMN, SRMP, 91191 Gif-sur Yvette, France
e-mail: maylise.nastar@cea.fr

D. Monceau
Institut Carnot CIRIMAT ENSIACET, 4 allée Emile Monso, BP 44632,
31030 Toulouse Cedex 4, France
e-mail: daniel.monceau@enisacet.fr

Keywords Oxidation · Vacancies · Annihilation · Voids

Introduction

On Voids Formation During High Temperature Oxidation

Oxide scale growth at high temperature is sometimes accompanied by a void formation beneath the metal/oxide interface within the metal. This phenomenon has been reported for example in several studies concerning high temperature oxidation of Ni-based alloys forming a chromia scale. In most cases, the depth of chromium depletion measured from the alloy–scale interface is similar to the corresponding depth of void penetration from that interface [1–4]. Shida et al. [2] showed that voids appear within metal grains as well as at grain boundaries. In Douglass [5] and Hales and Hill [6] studies, most of the voids lie at metal grain boundaries. ODS alloys are not exempted of voids and Rosenstein et al. [3] together with Weber and Gilman [4] showed that void formation in ODS alloy is not dependent on the presence of oxide dispersions. Recently, Aublant et al. [7] evidenced the influence of the cold-work on the density of voids formed beneath the oxide scale in Ni–20Cr–10Fe alloy. Figure 1 shows examples of voids formation. It compares one mirror polished sample—1 μm diamond paste finishing (Fig. 1b) with a SiC P1200 grinded sample (Fig. 1a) showing that the polished sample exhibits a higher density of voids that the ground one [7]. Figure 1c shows a cross section observation of Ni–30Cr oxidized at 1200 °C during 100 h [3].

Other systems that are also well known to be subjected to void formation during high temperature oxidation are the alumina forming intermetallics NiAl, FeAl and Ni3Al [8]. The cavities developed at β-NiAl/Al_2O_3 interface are observed even in the very early stages of reaction [9]. The addition of platinum to the intermetallic decreases both their size and density, whether or not sulfur is present in the alloy [10].This decrease in void volume fraction is not due to decrease in aluminium consumption by oxidation since alumina scaling rates are accelerated by the presence of platinum [11].

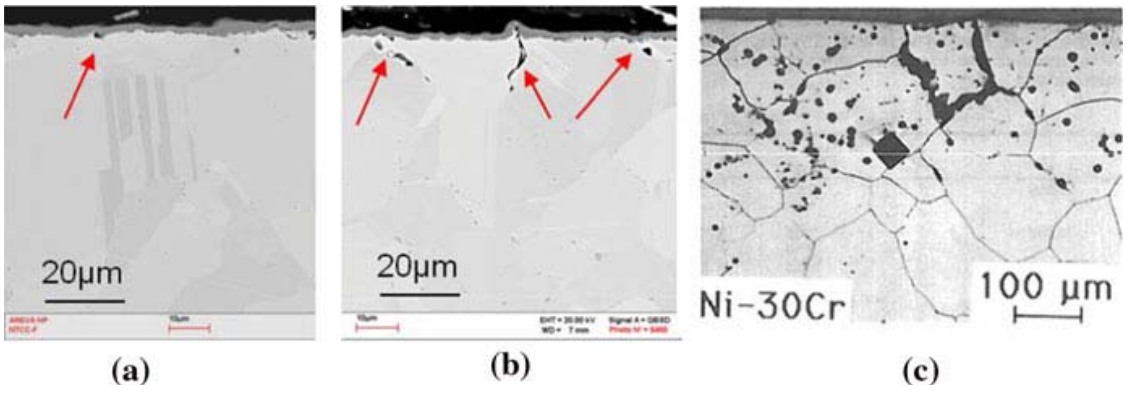

Fig. 1 Voids on Ni–20Cr–10Fe oxidized in air at 900 °C during 1,500 h by Aublant et al. [7]. **a** On a SiC P1200 grit ground sample; **b** on a mirror polished sample; **c** from Rosenstein et al. work [3] on a Ni–30Cr model alloy after oxidation in air at 1200 °C during 100 h

Sources of Vacancies: Cationic Injection and Kirkendall Effect

Evans [12] has listed the various origins of cavitation phenomena during high temperature oxidation. The most frequent mechanism advanced is the vacancy supersaturation leading to void formation by nucleation mainly on singularities such as grain boundaries. The sources and sinks of vacancies in high temperature processes are well identified.

First, the growth of an external scale by outward metal transport means that new oxide is formed at the scale–gas interface, and cannot fill the space vacated by the reacted metal. In fact, it is assumed that cationic vacancies are injected at the scale–metal interface, as metal atoms are transferred into the scale as cations. Pieraggi et al. [13] have linked the capacity of interfaces to annihilate these incoming vacancies to the ability of interface dislocations to climb. In the case of oxide scales growing by cations transport only, they showed that cationic vacancies could only be annihilated by climbs of disorientation or misfit dislocations in the metal, these latter being energetically favored. However detailed observations made by Francis and Lees [14] on pure iron and later by Perusin et al. [15] on pure nickel prove that a part of vacancies can migrate inside the metal bulk. Hence, this later study estimates from a 1 mm thick sample, oxidized on one face only at 1,000 °C during 48 h, that 0.38 % of vacancies formed during oxidation are injected in the metal and cross the entire sample to be annihilated at the opposite non-oxidized surface. When the same metal is oxidized in the same conditions on both faces, 0.01 vol% of cavities are observed inside the sample at the grain boundaries. These voids correspond approximately to the same fraction of injected vacancies.

Secondly, alloys are subjected to an additional effect, arising from the mismatch in the mobilities of the constituent metals. In fact, since the evidence of the role of vacancies in the diffusion process, proposed in 1942 by Seitz's and co-authors [16] through activation energy calculations, and independently proven the same year by Kirkendall [17] using a diffusion couple experiment, it is known that the mismatch between the diffusion coefficients of two diffusing elements leads to a vacancy flux in the opposite direction of the flux of the fastest element. This vacancy flux equals the opposite of net sum of fluxes of all the species that migrate on substitutional sites of the crystal via vacancy exchange mechanism, when expressed in the reference frame of the crystal lattice. Since the historical Kirkendall's experiment on the interdiffusion between copper and zinc in brass, the phenomenon has been evidenced on various systems with strong differences in diffusion coefficients of the system components. During the high temperature oxidation process, fluxes of species are driven by the chemical potential gradients arising from the concentration profiles in the alloy, and the selective oxidation of one element can lead to conditions near the metal oxide/interface very similar to an interdiffusion couple when considering the depletion profile. Hence, the Kirkendall effect will be effective and will act as a second source of vacancies in the case of alloy oxidation leading to subsequent depletion in alloying element near the interface. Besides, it is interesting to notice that the direction of the Kirkendall vacancy flux can either be raised from the metal/oxide interface to the metal bulk or in the opposite direction, depending on the selective oxidized element being the fastest or the slowest

diffusing species in the alloy. Hence, as shown on Fig. 2, in the case of β-NiAl (Al < 50 %) oxidation, Al diffuses slower than Ni and the Kirkendall vacancy flux rises from the alloy bulk towards the metal/oxide interface, leading to growing pores under the oxide scale. Whereas in the case of Ni–Cr alloys forming chromia scales, the Kirkendall flux rises from the metal/oxide interface towards the alloy bulk, since Cr diffuses much faster than Ni, leading to pores formation in the bulk of the alloy.

If vacancies are all annihilated at sinks like dislocations, they do not cause void formation within the metal, but nonetheless the reacting metal shrinks and this strain needs to be accommodated on some sample surface. If sinks are not efficient enough, a classic condensation model can be applied to anticipate voids formation in the presence of an oversaturation of vacancies. The location of the voids depends on the precise transport mechanisms in effect. In addition, new vacancies can also be emitted from dislocations in the reverse of the annihilation process, in regions where vacancies are under-concentrated with respect to their equilibrium value.

In addition to void formation, other effects can be linked to the transport of vacancies in the substrate beyond the oxide scale. In particular, a strong affinity between vacancies and some impurity atoms would cause the impurity atoms to diffuse together with vacancies, rather than in an opposite direction. This is the so-called drag effect. The driving force for this solute atom diffusion is dominated by cross-term coefficients in the diffusivity matrix. Some growth scale mechanisms are also strongly correlated with vacancies injection. For example, in the available space model mechanism for duplex scales, one considers that none of the incoming vacancies arising from the cationic growth of the external scale are annihilated, and that the anionic growth of the internal scale is controlled by the space occupied by the injected vacancies filling with anions [18].

Oxidation Modeling Taking into Account Vacancies Sources and Sinks

For a cationic transport mechanism in the oxide scale, most models based on Wagner's theory consider that all the vacancies are annihilated at the metal/oxide interface. Hence, the interface motion relative to the metal lattice is straightforwardly deduced from the quantity of metal consumed by the oxide growth, and as a result it is linked to the parabolic growth kinetics. Gesmundo and Hou [19] have proposed a theoretical analysis of void formation kinetics at the FeAl/Al_2O_3 interface, taking into account the vacancy flux from the Kirkendall effect in the

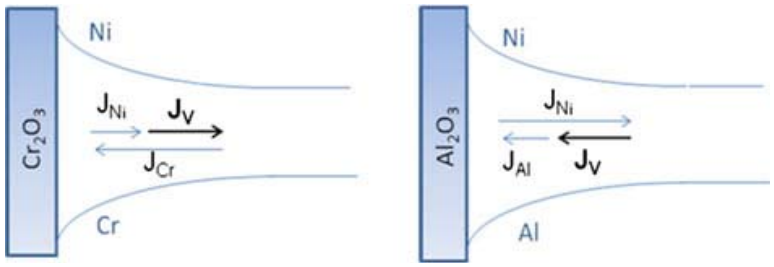

Fig. 2 Schematic of vacancy Kirkendall flux: in the case of NiCr alloys (*left*) and in the case of NiAl with Al content <50 % alloys (*right*)

alloy (due to the large difference between Al and Fe diffusivities) and the vacancy flux due to the cationic oxide growth. This later model assumes an immobile interface and that all the vacancies reaching the interface condensate to form voids. Nevertheless, in most cases, it would be more appropriate to consider that vacancies are neither all eliminated at interface nor all injected in the metal, but rather partially annihilated at the interface and hence partially injected in the metal. Moreover the oversaturated vacancies may also be annihilated in the bulk by dislocation climbs. Bobeth et al. [20] has proposed an analytical treatment to take into account the elimination of vacancies both at the metal/oxide interface movement and at distributed sinks in the bulk. Nevertheless, he considers the flux of vacancies injected by outward oxide growth mechanism only and not the Kirkendall flux inside the alloy. Additionally, even if the vacancy oversaturation was too small to induce the precipitation of voids, it would strongly increase the atom diffusivities and then modify the depletion profile and the creep rate in the alloy [21]. To investigate these phenomena, a numerical model has been implemented in the model EKINOX, to deal with the kinetics of vacancy annihilation at the metal/oxide interface but also in the bulk.

Aim of the Paper

Firstly, after a description of the numerical model, EKINOX is applied to the specific case of a Ni–30Cr alloy oxidized at 1,273 K. The kinetics of both the oxide scale and the Cr depletion profile in the alloy are described. Second, EKINOX calculations are used to study the influence of dislocation distribution on the vacancy profile evolutions in the substrate and on Cr depletion profile by considering two cold work conditions: High cold worked (HCW) and low cold worked (LCW). Then, the effect of a vacancy supersaturation on the precipitation of voids is discussed by means of the classical nucleation theory.

EKINOX Model

Fundamental Diffusion Equations

The EKINOX model is based on a set of equations using classical diffusion equations, vacancy elimination/creation equation, and interface reaction equations at moving boundaries. The concentration profile evolution is calculated both for chemical species and for vacancies in the alloy and in the oxide, and the oxide scale growth is also an output of the simulation. This set of differential equations is solved on a 1D mesoscopic discretization of the space. The time evolution of the local concentrations of the different species is computed using an explicit finite differential algorithm. A specific algorithm is used to simulate the interface displacement (metal/oxide and oxide/media) over large scale. The equations used have been presented in details in previous papers that presented EKINOX calculations for pure nickel oxidation [22, 23]. Hence in this part of the present

paper, a short description of the model is given only. Instead, we present in details the diffusion model of the Ni–Cr alloy.

Mesoscopic Space Discretization and Vacancy Treatment

The numerical model EKINOX is implemented in a 1D geometry of the concentration fields. It simulates the growth of a pre-existing thin external oxide layer whose composition is MOγ. To solve the set of equations of the model the space is divided into N_s slabs. In every slab, the concentrations are assumed to be uniform. Diffusion is controlled by a vacancy diffusion mechanism and atomic fluxes between two successive layers are assumed to be proportional to the concentration gradients following the first Fick's law. Considering that the vacancy exchange mechanism as the only diffusion mechanism, the vacancy flux from one slab to the other is directly calculated as the opposite of the sum of fluxes of the chemical species. The substrate (i.e., the alloy) extends from the N_1 slab to the N_ith slab and the oxide scale extends from the slab N_{i+1} to the slab N_s. In the oxide, two distinct sub-lattices are considered for the cations and for the anions, whereas only one lattice is considered in the metal. Each sublattice is occupied either by the corresponding chemical species (metal M, oxygen O) or by the corresponding vacancies (V_M, V_O). The model can either consider pure anionic growing scales, pure cationic growing scales or mixed growing scales. In the present calculations the chromia scale has been considered to grow by a pure cationic mechanism leading to a maximum injection of vacancies in the alloy. Many of the early data on Cr_2O_3 scale growth rates and mechanisms have been reviewed by Kofstad [24]. Although the defect properties of Cr_2O_3 are not fully understood, he concluded that chromia scales grow mainly by outward diffusion of chromium.

In the metallic substrate, vacancies are treated as non-conservative species: the total amount of vacancies evolves during the simulation. They can be eliminated in the substrate by dislocations and at the metal/oxide interface by misfit dislocations between the oxide and the substrate. Following the model developed in [23], the rate of the vacancy concentration variation is given by Eq. 1 where ρ_n refers to the dislocation density in the slab n, and leads to the decrease of the corresponding layer thickness (see [21]):

$$\left.\frac{\partial X_V^n}{\partial t}\right|_{sinks} = -\frac{\rho^n}{\Omega^n}\left(X_{eqV}^n - X_V^n\right) \tag{1}$$

where X_{eqV}^n and X_V^n respectively refer to the equilibrium concentration and effective vacancy concentration. This equation is integrated together with the Fick's first law using the finite difference algorithm.

Adaptation to the Diffusion in Ni–Cr Alloys: Derivation from the Atomic Scale

To calculate diffusion fluxes in the substrate, diffusion coefficient are derived from an atomic diffusion model. In the alloy, diffusion is controlled by atom-vacancy exchange frequencies which depend on temperature and local composition of the

alloy through thermodynamic and kinetic parameters of a "broken bond" model. The frequencies satisfy the detailed balance which guarantees a coherent treatment of kinetics and thermodynamics.

The diffusion coefficients of Ni–Cr alloys are deduced from the atomic diffusion model by using the self-consistent mean field method. The resulting diffusion coefficients depend on local concentration. The atomic diffusion model of Ni–Cr alloys has been validated on different alloy compositions and is now suitable even for Ni-base ternary alloys: Ni–Fe–Cr [25]. Thus diffusion coefficients (Eq. 4) are not extrapolated from high temperature instead they are calculated from the mean exchange frequencies and differences between energy contributions at the saddle point and the stable point (Eq. 3), both expressed in terms of nearest neighbor pair interaction energies [25]: ε_{ij}, for stable point and ε_{ij}^{sd} for saddle point with i or j = Ni, Cr, V whose values are given in Table 1. Together with the pre-exponential factor for the atomic exchange mechanism, D_i^0 given in this Table 2, the final model reaches a good agreement with the tracer diffusion experimental data, for binary Ni–Cr alloys as shown in [23]. It predicts that the mean exchange frequencies of Cr and Ni should stay on a ratio around three at any composition, even at low temperatures [25]. Hence, the chemical potential in Eq. 4, that defined the diffusion coefficient matrix, is directly calculated as the second derivative of the free energy F per atom which is assumed to be the one of a regular solution model:

$$F = \frac{Z}{2} \sum_{i,j=\mathrm{Ni,Cr,V}} X_i X_j \varepsilon_{ij} + k_B T \sum_i X_i \log(X_i) \tag{2}$$

where ε_{ij} is the pair interaction energy between species i and j, k_B is the Boltzmann constant, Z the coordination number and T the temperature and X_i the concentration of i in site fraction.

The activation energy is deduced from the broken bond model:

Table 1 Pair interaction energy model and saddle point model for Ni–Cr alloy

Pair ij	ε_{ij} (eV)	ε_{ij}^{sd} (eV)
NiNi	−0.74	−2.6
CrCr	−0.71	−2.5
NiCr	−0.763	−2.66
CrV	−0.2167	
NiV	−0.2225	

Table 2 Input kinetics parameters

i	D_i^0 (cm^2 s^{-1}) for Ni–Cr Alloy	(z + 1)D_{Vi} (cm^2 s^{-1}) for Cr_2O_3 at 1,273 K
Ni	2.3	
Cr	7.0	1.08×10^{-7}

$$E^{act}_{i=\mathrm{Ni,Cr}} = \sum_{j=\mathrm{Ni,Cr,V}} X_j \varepsilon^{sd}_{ij} - \sum_{j=\mathrm{Ni,Cr,V}} X_j(\varepsilon_{ij} + \varepsilon_{Vj}) \tag{3}$$

where ε^{sd} is the interaction at the saddle point. The resulting diffusion coefficient is equal to:

$$D^n_{ij=\mathrm{Ni,Cr}} = D^0_i X^n_V X^n_i \exp\left(-\frac{E^{act}_i}{kT}\right) \frac{\partial(\mu_i - \mu_V)}{\partial X_j} \tag{4}$$

Initial Conditions

For the present calculations, the homogeneous composition of Ni–30Cr type alloy is considered to be corresponding to 32.6 at.% of Cr. The initial concentration of vacancies in the metal, the initial concentration is also taken constant at the value of the equilibrium concentration. The vacancy formation energy is directly calculated from pair interaction energies given in Table 1. Since the numerical model does not enable to start the calculation with no pre-existing scale, an initial oxide scale is assumed to be present at the initial time of the calculation. All the calculations have been performed with $N_s = 103$ with three oxide slabs as initial system corresponding to a total thickness of 50 μm, and to an initial chromia oxide scale of 1.5 μm thick. The cationic vacancy concentrations at the interfaces of the chromia oxide scale are taken constant during the calculation with values given in Table 3.

In the metal, the densities of sources and sinks of vacancies are assumed to be non-uniform. To reproduce the condition of a cold-worked surface, a higher density of sinks (ρ_{surf}) is attributed to the slabs corresponding to the substrate just beneath the oxide scale with decrease towards the sink density of the bulk alloy (ρ_{bulk}) following a linear law. The depth affected by this higher density of sinks (d_{CW}) is chosen to be 10 μm thick. Furthermore, since the metal/oxide interface is a very efficient sink, a very high local density (ρ_{int}) of sinks is considered to be linked to this interface. Hence, the density of sources and sinks for vacancies in the alloy can be described following the representation given in Fig. 3. These input data will be locally used in the Eq. 1 that governs the elimination or creation of vacancies in each slab. For the metallic slab N_i situated just beneath the oxide, both ρ_{int} and ρ_{surf} are included in the vacancy elimination equation. To compare the influence of these parameters on the results of the calculations, two sets of cold worked conditions have been investigated. They are presented in Table 4. They are referred as HCW and LCW conditions. Notice that, considering that the most effective sinks for vacancies are the dislocations climbs, values for these parameters have been chosen based on reported dislocation densities.

Table 3 Equilibrium concentration in chromia (site fraction)

$[V_{Cr}]^{oxide/gas}$	$[V_{Cr}]^{M/O}$
6.3×10^{-5}	1.0×10^{-6}

Results and Discussion

Oxidation Kinetics and Cr Depletion

Figure 4 illustrates the calculated scale growth kinetics for a 5 h oxidation at 1,273 K. The growth kinetics follows a parabolic law with a parabolic rate constant of $k_p = 1.33 \times 10^{-11}$ cm^2 s^{-1}, close to the value reported in the literature [26] and in accordance with the value calculated for steady state hypothesis:

$$k_p = 2(z+1)D_{V_{Cr}}\left(\left[V_{Cr}^{+z}\right]^{oxide/gas} - \left[V_{Cr}^{+z}\right]^{metal/oxide}\right) \quad (5)$$

where z in the charge of the vacancy.

Chromium and Vacancy Concentration Profiles

The Fig. 5a presents the Cr depletion profile in the alloy at various times along the simulation for the HCW conditions. Because of the relatively large initial oxide scale whereas the initial chromium concentration is homogeneous, an artificial transient stage appears before the establishment of the steady state for the Cr concentration profile in the metal and at the metal/oxide interface. Vacancy concentration profiles in the metal (Fig. 5b) exhibits an oversaturation near the metal/oxide interface at 30 min. Then it decreases and reaches a plateau as the vacancies diffuse deeper in the alloy, a large concentration peak arises inside the alloy at a depth corresponding to the non cold-worked part of the alloy. This peak increases and enlarges with The first peak which appears near the metal oxide interface during the shortest times can be attributed to the vacancies injection due to the cationic growth of the chromia scale, whereas the oversaturation peak inside the alloy that developed for longer time is attributed to the Kirkendall effect. In fact, it appears when the Cr depletion profile

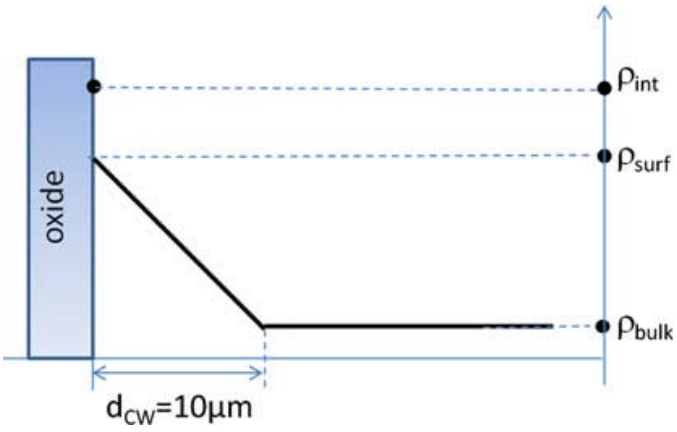

Fig. 3 Profile of dislocation density in the substrate, used as input parameter for the density of sinks and sources of vacancies

Table 4 Input parameters for cold worked state that characterize the efficiency of vacancies sources and sinks

Cold work conditions	ρ_{int} (cm^{-2})	ρ_{surf} (cm^{-2})	ρ_{bulk} (cm^{-2})
HCW	10^8	10^6	10^4
LCW	10^8	10^5	10^4

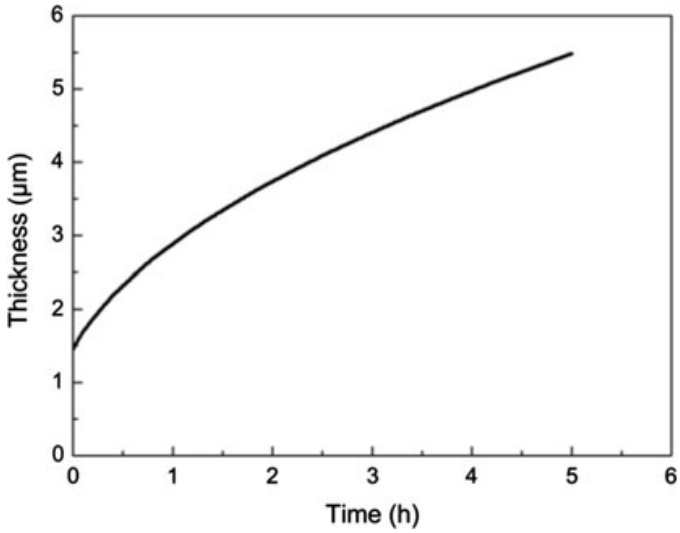

Fig. 4 Calculated growth scale kinetics for Ni–30Cr alloy oxidized 5 h at 1,273 K

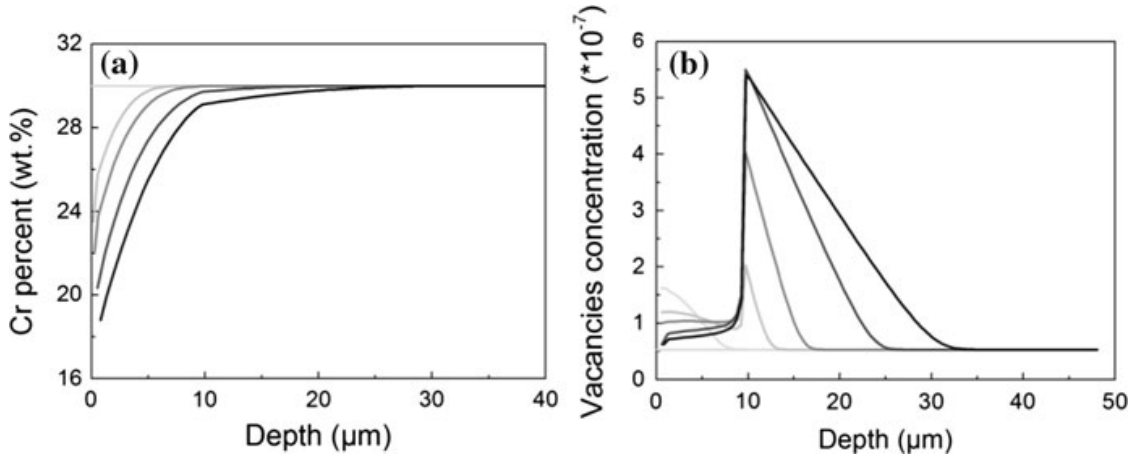

Fig. 5 Calculation of the evolution of the Ni–30Cr alloy along the oxidation at 1,273 K during 5 h at various times (30 min, 1 h, 1 h 30 min, 3 h, 5 h from *light gray line* to *black line*) of the simulation. **a** Cr depletion profile in the alloys and **b** vacancy profile inside the alloy

reaches the non cold worked part of the alloy. The reason for this development is that the density of sinks in this part of the alloy is not sufficient to compensate the vacancy flux due to Kirkendall effect (higher Cr flux compared to Ni flux) leading to an oversaturation rising in this part. Hence, the shape of vacancy profile in the substrate is considerably different from the case of oxidation of pure nickel presented in previous work [23] that exhibited an oversaturation of vacancies only due to cationic vacancies injection with a continuous decrease from the metal/oxide interface to the bulk. The shape of this profile in case of NiCr alloy is in good accordance with that of the volume fraction of voids as a function of depth for the Inconel alloy after long time oxidation reported by Rosenstein et al. [3].

Effect of Cold Working

This non-monotone concentration profile for vacancies affects the diffusion of the species since the diffusion coefficients depend locally on the vacancy concentration

(Eq. 4). Hence, one can see on the Cr depletion profile calculated for the longer time (5 h), that the Cr depletion profile exhibits a "broken shape" at the limit of the cold worked zone. This corresponds to the Kirkendall vacancies oversaturation peak that enhances diffusion in this region.

For a better understanding of the role of cold working conditions, comparison of calculations for HCW and LCW conditions is shown in Fig. 6. A cold worked depth of 10 μm is considered in both cases. The conditions only differ by the density of sinks in the cold worked region. Profiles at the end of the simulation (5 h of oxidation) for both conditions are respectively represented in Fig. 6a, b. Cold working conditions affect the Cr depletion profile in a significant manner. They modify both the Cr depletion depth and the chromium concentration at the interface. For the LCW conditions, the lower density of sinks for the vacancies leads to a higher oversaturation of vacancies compared to the HCW case, in particular in the cold-worked region. Consequently in the case of LCW, the diffusion is enhanced and the Cr depletion depth is larger than in the HCW conditions for which the oversaturation of vacancies is lower. Correspondingly, the Cr concentration at the interface is higher for the LCW conditions, because the alloy supplies more Cr to the metal/oxide interface. This effect has been also reported in the experimental study [7], comparing depletion profile depth for the grinded sample and the finished sample.

Void Formation

In the present simulations, after 5 h of oxidation, the maximum supersaturation of vacancy reaches approximately 10. From the classical nucleation theory, we know that the nucleation barrier as well as the critical radius for the vacancy aggregate to be stable decrease with respect to the vacancy supersaturation. Considering pure Ni data for an estimation of the surface energy (1.96×10^{-4} J cm^{-2}) and the atomic volume, a vacancy supersaturation equal to 10 yields a nucleation barrier of about 100 eV and a critical radius of nucleation of about 2 nm. To quantify the number of

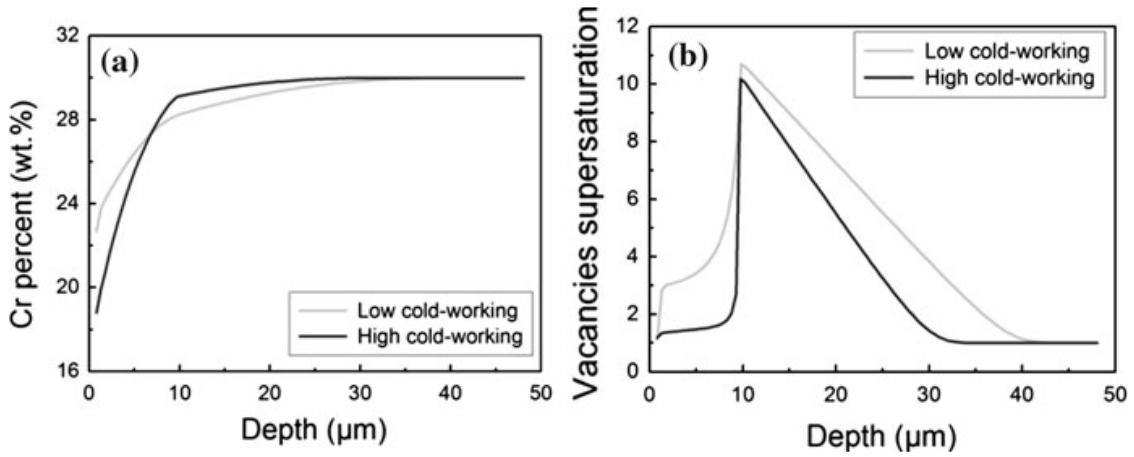

Fig. 6 Comparison of the Ni–30Cr alloy evolution for HCW case and the LCW case for 5 h oxidation at 1,273 K. **a** Cr depletion profiles and **b** vacancy concentration profiles

formed voids, it is possible to calculate the nucleation rate. It shows that a supersaturation of 10 is not sufficient to form pores of visible size. This is in agreement with experimental results showing that the pores appear on SEM observations at longer times than 5 h.

Conclusions

During high temperature oxidation of alloys, two kinds of vacancies sources can be active and concomitant with scale growth: vacancies injection from the metal/oxide interface and Kirkendall flux. Sinks, such as dislocations with a distribution arising from the cold working state in the metal, contribute to annihilate the oversaturated vacancies. To investigate the balance between these three phenomena on vacancies concentration profile inside the alloy, the EKINOX numerical code has been adapted to Ni–Cr alloy oxidation. Hence, simulations in the case of a Ni–30Cr alloy for 1,273 K oxidation have been performed. The chromia scale growth kinetics is calculated and corresponding Cr depletion profile and vacancies profile inside the metal were analyzed for two cold-work conditions. Results show that the cold working state of the alloy strongly influences the Cr depletion profile. The evolution of the vacancy concentration profile with time exhibits the signatures of both vacancies sources: cationic injection for shortest times, and the arising of a Kirkendall vacancy flux at longer time, which is the dominant phenomenon in the present case. In fact, a sharp increase arises on the vacancies profile in the bulk region of the alloy as soon as the Cr depletion depth exceeds the cold worked depth and reaches the bulk region where the density of sinks is lower. This rise is attributed to Kirkendall flux due to the mismatch between Cr and Ni motilities. However, based on the classical nucleation theory, the oversaturation will not lead to pores formation for the calculated cases. It would be of interest to do the same kinds of calculations but for NiAl intermetallic, the direction of the Kirkendall vacancies flux being in opposite direction in the $NiAl/Al_2O_3$ system compared to the $NiCr/Cr_2O_3$ system.

Acknowledgments F. Delabrouille (EDF) for providing model alloys, P. Poisson and L. Guérin (AREVA) for SEM observations are gratefully acknowledged.

References

1. P. Berthod, *Oxidation of Metals* **64**, 2005 (235).
2. E. Y. Shida, G. C. Wood, F. H. Stott, D. P. Whittle and B. D. Bastow, *Corrosion Science* **21**, 1981 (581).
3. A. H. Rosenstein, J. K. Tien and W. D. Nix, *Metallurgical Transactions A* **17A**, 1986 (151).
4. J. H. Weber and P. S. Gilman, *Scripta Metallurgica* **18**, 1984 (479).
5. C. D. L. Douglass, *Corrosion Science* **8**, 1968 (665).
6. R. Hales and C. Hill, *Corrosion Science* **12**, 1972 (843).
7. E. Aublant, O. Calonne, and M. Foucault, PTCMC-F R 11 0020 internal AREVA report.
8. D. J. Young, *High Temperature Oxidation and Corrosion of Metals*, (Elsevier, Amsterdam, 2008).
9. D. Oquab and D. Monceau, *Scripta Metallurgica* **44**, 2001 (2741).
10. B. Gleeson, W. Wang, S. Hayashi and D. Sordelet, *Material Science Forum* **461–464**, 2004 (213).

11. Y. Cadoret, D. Monceau, M.-P. Bacos, P. Josso, P. Marcus and V. Maurice, *Oxidation of Metals* **64**, 2005 (185).
12. H. E. Evans, *Materials Science and Technology* **4**, 1988 (1089).
13. B. Pieraggi, R. A. Rapp and J. P. Hirth, *Oxidation of Metals* **44**, 1995 (63).
14. R. Francis and D. G. Lees, *Materials Science and Engineering* **120**, 1989 (97).
15. S. Perusin, B. Viguier, D. Monceau, L. Ressier and E. Andrieu, *Acta Materiala* **52**, 2004 (5375).
16. H. B. Huntington and F. Seitz, *Physical Review* **61**, 1942 (315).
17. E. O. Kirkendall, *Transaction the Metallurgical Society of AIME* **147**, 1942 (104).
18. L. Martinelli, F. Balbaud-Célérier, A. Terlain, S. Bosonnet, G. Picard and G. Santarini, *Corrosion Science* **50**, 2008 (2537).
19. F. Gesmundo and P. Y. Hou, *Oxidation of Metals* **59**, 2003 (63).
20. M. Bobeth, M. Gutkin, W. Pompe and A. E. Romanov, *Physica Status Solidi A* **165**, 1998 (165).
21. S. Dryepondt, Y. Zhang and B. A. Pint, *Surface and Coating Technology* **201**, 2006 (3880).
22. C. Desgranges, N. Bertrand, K. Abbas, D. Monceau and D. Poquillon, *Material Science Forum* **461–464**, 2004 (481).
23. N. Bertrand, C. Desgranges, M. Nastar, G. Girardin, D. Poquillon and D. Monceau, *Material Science Forum* **595–598**, 2008 (463).
24. P. Kofstad, *Oxidation of Metals* **44**, 1995 (3).
25. V. Barbe and M. Nastar, *TMS Letters*, Vol. 2 (TMS, The Minerals, Metals and Materials Society, Warrendale, 2005), p 93.
26. C. S. Giggins and F. S. Pettit, *Transactions of the Metallurgical Society of AIME* **245**, 1969 (2495).